



Article

Mineral chemistry and genesis of monazite-(Sm) and monazite-(Nd) from the Blue Beryl Dyke of the Julianna pegmatite system at Piława Górna, Lower Silesia, Poland

Diana Twardak¹ , Adam Pieczka² , Jakub Kotowski³ and Krzysztof Nejbert³

¹University of Gdańsk, Faculty of Oceanography and Geography, Division of Marine Geology, 81-378 Gdynia, Piłsudskiego 46, Poland; ²AGH University of Science and Technology, Department of Mineralogy, Petrography and Geochemistry, 30-059 Cracow, Mickiewicza 30, Poland; and ³University of Warsaw, Faculty of Geology, 02-089 Warsaw, Żwirki and Wigury 93, Poland

Abstract

Monazites are one of the most interesting groups of accessory mineral components of crystalline rocks due to the information on geochemical evolution of the crystallisation environment coded in their chemical compositions, in addition to comprising one of the most valuable objects for geochronology studies. This paper presents monazite-(Sm) and monazite-(Nd) from the Blue Beryl Dyke of the Julianna system of rare-element pegmatites at Piława Górna, Lower Silesia, Poland. These monazites are unique due to their unusually high Sm and Nd contents, reaching 33.22 wt.% Sm₂O₃ and 34.12 wt.% Nd₂O₃, respectively. We consider the most significant factors of the enrichment in Sm and Nd to be the occurrence of highly fractionated pegmatite-forming melts during the final stages of solidification and associated hydrothermal fluids that were strongly enriched in rare earth element REE–Cl and REE–F complexes. Local disequilibria allowed for the rapid growth of accessory phases under supercooling conditions associated with the scavenging of selected elements, leading to their local depletion, which was not balanced by diffusion processes. As a consequence, the depletion of light rare earth elements (LREE) led to the incorporation of available middle rare earth elements (MREE, Sm–Dy) in the case of Sm and Nd, which could occupy an acceptable structural position in minerals of the monazite group.

Keywords: monazite-group minerals, monazite-(Sm), monazite-(Nd), REE distribution patterns, tetrad effect, rare-element pegmatites

(Received 2 February 2023; accepted 17 May 2023; Accepted Manuscript published online: 29 May 2023; Associate Editor: Sam Broom-Fendley)

Introduction

The monazite group consists of monoclinic orthophosphates of the APO₄ type of light rare-earth elements (LREE: La–Gd), Th, and Ca, crystallising with a *P21/n* space-group symmetry with nine-fold coordinated A cations. This group includes monazite-(La), monazite-(Ce), monazite-(Nd), monazite-(Sm), monazite-(Gd) and cheralite (Levinson, 1966; Graeser and Schwander, 1987; Masau *et al.*, 2002; Linthout, 2007; Ondrejka *et al.*, 2023). Monazite-(Ce) is a common accessory mineral in granitic igneous and gneissic metamorphic rocks, and also occurs in detrital sands derived from such crystalline rocks. Monazite-(La) and monazite-(Nd) are much rarer, whereas monazite-(Sm) and especially monazite-(Gd), are extraordinarily rare, growing only in specific magmatic and post-magmatic environments.

Among the rarer varieties of monazite, monazite-(Nd) is more common and its occurrence has been described in gneisses,

carbonatites, sandstones, metamorphic magnetite ore deposits, and veins associated with hydrothermal mineralisation (Graeser and Schwander, 1987; Del Blanco *et al.*, 1998; Kusiak and González-Álvarez, 2006; Pršek *et al.*, 2010; Števkó *et al.*, 2014; Mitchell and Smith, 2017; Ondrejka *et al.*, 2023). Monazite-(Sm) has only been described in a pod of lepidolite-subtype granitic pegmatite from the Annie Claim #3 pegmatitic leucogranite, which is part of the Greer Lake intrusion in south-eastern Manitoba (Masau *et al.*, 2002), and as a phase accompanying monazite-(Gd) in a REE–U–Au hydrothermal quartz vein in the Western Carpathians, Slovakia (Ondrejka *et al.*, 2023). Monazite-(Nd) occurs mostly as crystals with an average of >12 to up to ~25 wt.% Nd₂O₃. Two known exceptions include monazite-(Nd) containing 30.32 wt.% Nd₂O₃ (0.44 Nd atoms per formula unit; apfu) (Graeser and Schwander, 1987) and monazite from sandstones belonging to the Grinnell Formation at Red Rock Canyon in the Waterton–Glacier International Peace Park, south-western Alberta, Canada, mentioned by Kusiak and González-Álvarez (2006) as containing up to 31 wt.% Nd₂O₃ (0.45 Nd apfu). The Sm₂O₃ contents of monazite-(Sm) are known to be relatively low. Masau *et al.* (2002) reported only up to 14.29 wt.% Sm₂O₃ (0.197 Sm apfu) in the holotype monazite-(Sm) while Ondrejka *et al.* (2023) measured

Corresponding author: Adam Pieczka; Email: pieczka@agh.edu.pl

Cite this article: Twardak D., Pieczka A., Kotowski J. and Nejbert K. (2023) Mineral chemistry and genesis of monazite-(Sm) and monazite-(Nd) from the Blue Beryl Dyke of the Julianna pegmatite system at Piława Górna, Lower Silesia, Poland. *Mineralogical Magazine* 87, 575–581. <https://doi.org/10.1180/mgm.2023.38>

© The Author(s), 2023. Published by Cambridge University Press on behalf of The Mineralogical Society of the United Kingdom and Ireland. This is an Open Access article, distributed under the terms of the Creative Commons Attribution licence (<http://creativecommons.org/licenses/by/4.0/>), which permits unrestricted re-use, distribution and reproduction, provided the original article is properly cited.

Sm₂O₃ contents of 17.32 wt.% (0.236 Sm apfu) in monazite-(Sm) and up to 17.68 wt.% Sm₂O₃ (0.241 Sm apfu) in monazite-(Gd).

Monazite-group minerals and xenotime-(Y) are common accessory minerals in the anatectic pegmatite bodies of the Julianna system at Piława Górna in Lower Silesia, Poland (Szuszkiewicz *et al.*, 2013). The monazite occurrences are almost exclusively represented by monazite-(Ce) with varying compositions, however individual crystals of monazite-(Nd) and monazite-(Sm) have been encountered in one vein, described as the Blue Beryl Dyke. The main aim of this contribution was to document their occurrence and clarify the reasons behind their atypically high Nd and Sm enrichment.

Geology and mineralogy of the Blue Beryl Dyke

The Julianna pegmatite system crops out in an active amphibolite-migmatite quarry (50.70327, 16.73677) at Piława Górna in the Góry Sowie Block (Szuszkiewicz *et al.*, 2013). The unit constitutes a central part of the Sudetes at the NE margin of the Bohemian Massif in SW Poland. The pegmatites crystallised from anatectic melts produced by partial melting of metasedimentary-metavolcanic rocks during retrograde amphibolite-facies metamorphism ca. 370–380 Ma (Van Breemen *et al.*, 1988; Timmermann *et al.*, 2000). Most of the anatectic melts were trapped in neosomes in migmatites, whereas the rest occur in pegmatite bodies located along tectonic zones in the Góry Sowie metamorphic rocks (Szuszkiewicz *et al.*, 2013; Pieczka *et al.*, 2015). The pegmatite system consists of a network of co-genetic dykes and vein- and nest-type apophyses that vary in size and degree of geochemical evolution and represent barren and rare-element pegmatites. They individually represent various subclasses that correspond to the niobium-yttrium-fluorine (NYF) and lithium-caesium-tantalum (LCT) petrogenetic families in the pegmatite classification of Černý and Ercit (2005), however overall, the system exhibits hybrid NYF + LCT characteristics. Wise *et al.* (2022) classified the Góry Sowie pegmatites as an example of type 1 DPA (direct product of anatexis) pegmatites, showing a typical Be-Nb-Ta-P-Li-B geochemical signature.

The Blue Beryl Dyke, which was exposed in 2010, extended over a few tens of metres horizontally with a maximum thickness of ~3–4 m. The zoning was typical up to the blocky unit with interstices among feldspars filled with quartz, but without a massive core. The characteristic features of the dyke were the presence of short prismatic crystals of pale-bluish low-Na,Cs beryl, abundant cassiterite and columbite-group minerals, and subordinate, few millimetre-sized, greenish crystals of gahnite associated with ferro- and zinconigerites-2N1S, (Al,Fe,Zn)₂(Al,Sn)₆O₁₁(OH) and (Zn,Al,Fe)₃(Al,Fe,Ti)₈O₁₅(OH), and -6N6S, (Al,Fe,Zn)₃(Al,Sn,Fe)₈O₁₅(OH) and (Zn,Al)₇(Al,Fe³⁺,Ti,Mg)₁₆O₃₁(OH), as well as genthelvite, Be₃Zn₄(SiO₄)₃S (Pieczka *et al.*, 2019). Tourmaline-supergrupp minerals were represented by Zn-enriched foitite, □(Fe²⁺Al)Al₆(Si₆O₁₈)(BO₃)₃(OH)₃(OH), evolving into schorl, NaFe₃²⁺Al₆(Si₆O₁₈)(BO₃)₃(OH)₃(OH); Li-bearing tourmalines were unique, occurring only as small dark greenish crystals of Fe-bearing elbaite, Na(Li_{1.5}Al_{1.5})Al₆(Si₆O₁₈)(BO₃)₃(OH)₃OH, and fluor-elbaite, Na(Li_{1.5}Al_{1.5})Al₆(Si₆O₁₈)(BO₃)₃(OH)₃F, in a few-centimetre-sized muscovite flakes, and as tiny inclusions in quartz and albite (Pieczka *et al.*, 2018). Lithium-bearing mineralisation was also represented by minute aggregates of spodumene, LiAlSi₂O₆, veinlets of a Cs-dominant dark mica, and single aggregates of partly altered lithiophilite, LiMn²⁺(PO₄), associated with ferrowodginite,

Fe²⁺Sn⁴⁺Ta₂O₈, and wodginite, Mn²⁺Sn⁴⁺Ta₂O₈. The REE-bearing phases were represented by rare to accessory monazite-(Ce), monazite-(Nd), monazite-(Sm), xenotime-(Y), allanite-(Ce) and traces of rhabdophane-group phosphates.

Methods

Electron-probe microanalyses of the monazite-group minerals from the Blue Beryl Dyke were performed at the Inter-Institute Analytical Complex for Minerals and Synthetic Substances at the University of Warsaw, Poland, with a CAMECA SX 100 electron microprobe. Wavelength-dispersive X-ray spectrometry was conducted under the following conditions: accelerating voltage of 15 kV, beam current of 70 nA, beam diameter of 2 μm, peak count-time of 20 s, and background times of 10 s before and 10 s after the peak. The following calibration materials (analytical lines, diffracting crystals, and mean detection limits in wt.% element) were used: diopside – Ca (Kα, PET, 0.01) and Si (Kα, TAP, 0.01); YAG – Y (Lα, PET, 0.03); LaP₅O₁₄ – La (Lα, PET, 0.02); CeP₅O₁₄ – Ce (Lα, PET, 0.03); PrP₅O₁₅ – Pr (Lβ, LIF, 0.06); GdP₅O₁₄ – Gd (Lα, LIF, 0.03); REE1 – Dy (Lβ, LIF, 0.16) and Er (Lα, LIF, 0.09); REE2 – Eu (Lβ, LIF, 0.15), Ho (Lβ, LIF, 0.16) and Tm (Lα, LIF, 0.13); REE3 – Sm (Lα, LIF, 0.09) and Yb (Lα, LIF, 0.07); REE4 – Nd (Lβ, LIF, 0.09), Tb (Lα, LIF, 0.10) and Lu (Lα, LIF, 0.15); galena – Pb (Mα, PET, 0.04); ThO₂ – Th (Mα, PET, 0.04); and UO₂ – U (Mβ, PET, 0.04), where REE1–REE4 are silica glass standards containing the respective lanthanides. The raw data were reduced with the PAP routine of Pouchou and Pichoir (1991). Corrections for interferences of REE lines were made on the basis of factors derived for the used microprobe considering the interferences indicated by Reed and Buckley (1998). The chemical formulae of monazite were normalised in relation to 4 O apfu. The REE-distribution patterns were normalised to the REE contents in CI chondrite (O'Neill, 2016). The decomposition of chondrite-normalised REE patterns was performed with the online interactive polynomial fitting using the *BlambdaR* application (Anenburg and Williams, 2022). This application allowed quantitative fitting on the estimated uncertainty for individual ln(REE) in percent (*s*) and the description of REE patterns through their decomposition into orthogonal polynomial functions (shape components) with coefficients known as the lambda coefficients (λ₀, λ₁, λ₂, λ₃, λ₄) and the tetrad effect coefficients (τ₁, τ₂, τ₃, τ₄), in addition to the calculation of statistically predicted REE_{λτ} concentrations.

Results

The single crystals of monazite-(Nd) (~10 μm in size) and monazite-(Sm) (~30 μm in size) found in the Blue Beryl Dyke were associated with columbite-group minerals that underwent alteration into fluor- to oxy/hydroxy-calcimicrolite and oxy/hydroxy-plumbomicrolite free of fluorine and were accompanied by more common monazite-(Ce). However, monazite-(Ce) was much less abundant than in other dykes of the pegmatite system, forming rare and disseminated minute grains, not more than several tens to 100 μm in size. Monazite-(Nd) occurred as an inclusion in columbite-(Fe) associated with more common inclusions of cassiterite, scheelite, uraninite and BiVO₄ (pucherite or clinobisvanite). Monazite-(Sm) formed an intergrowth with columbite-(Mn). Back-scattered electron (BSE) images of the monazites and the respective X-ray element maps depicting Ce, Nd, and Sm distributions in monazite-(Sm) are shown in Fig. 1. The grain of monazite-(Sm) is clearly heterogeneous with a visible

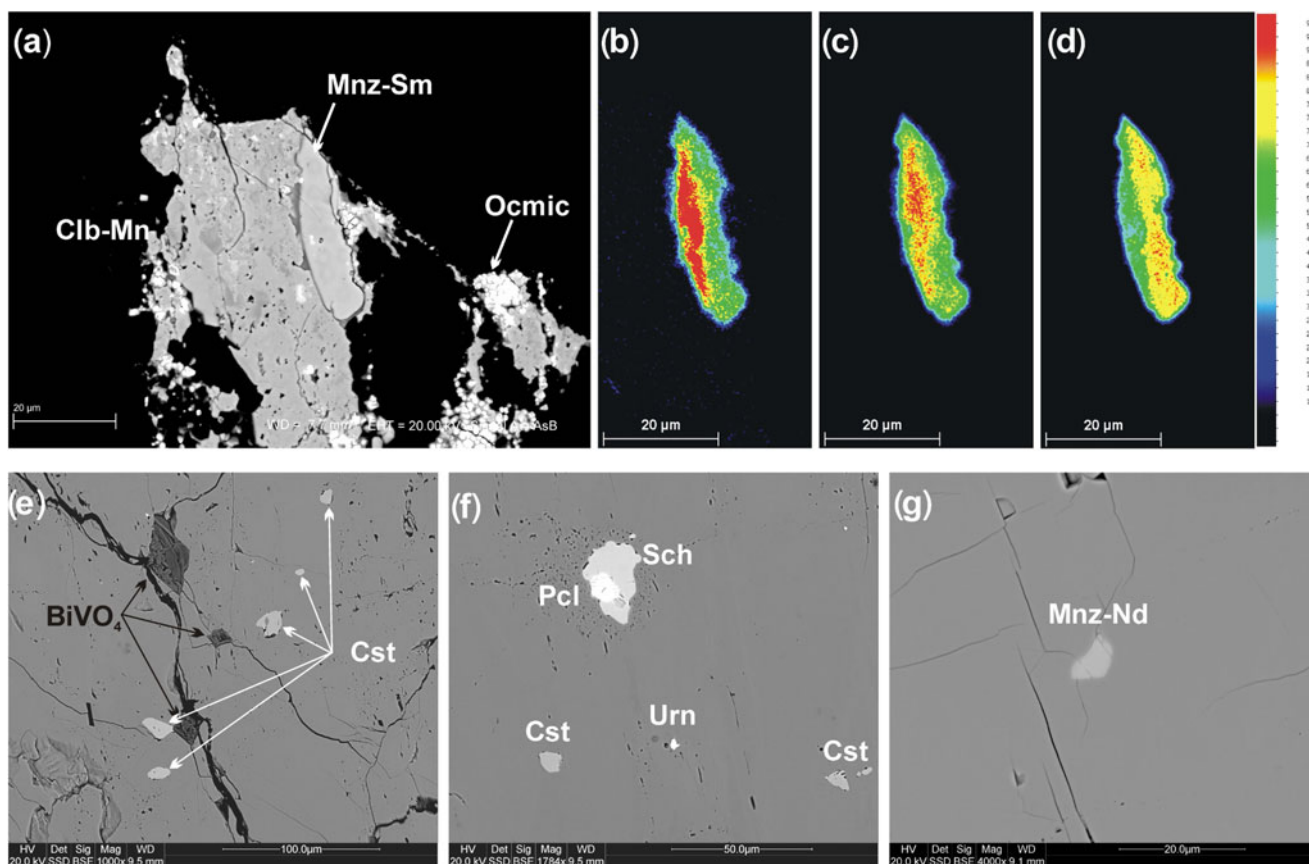


Figure 1. Mode of occurrence of monazite-(Sm) and monazite-(Nd) in the Blue Beryl Dyke: (a) BSE image of monazite-(Sm) intergrown with partly altered columbite-(Mn); dark field represents quartz and feldspars; (b,c,d) distributions of selected REE elements (Ce, Nd and Sm, respectively) within examined monazite-(Sm); (e–f) BSE images of inclusions of various phases in the columbite-(Fe) crystal containing monazite-(Nd); (g) an inclusion of monazite-(Nd) in the same columbite-(Fe). Symbols of mineral names from Warr (2021): Clb-Mn – columbite-(Mn), Cst – cassiterite, Mnz-Nd – monazite -Nd, Mnz-Sm – monazite-(Sm), Ocmic – oxycalciumicrolite, Pcl – a pyrochlore, Sch – scheelite, Urn – uraninite and BiVO₄ – pucherite or clinobisvanite.

correlation between Ce and Nd that were concentrated in different parts of the examined crystal to Sm, although the crystal was Sm-dominated overall. Representative electron-probe microanalyses of the three monazite species are presented in Table 1. The complete set of microprobe analyses of the dyke monazites is available as Supplementary Material (Table S1). The analysed monazite-(Ce) grains show diverse compositions evolving towards more enriched middle rare earth element (MREE, Sm–Dy) contents, including up to 0.272 Nd apfu (19.19 wt.% Nd₂O₃), 0.152 Sm apfu (11.07 wt.% Sm₂O₃), and 0.075 Gd apfu (5.61 wt.% Gd₂O₃). The increasing MREE contents reach their maximum concentration in monazite-(Nd) containing 0.486 Nd apfu (34.12 wt.% Nd₂O₃), 0.095 Sm apfu (6.90 Sm₂O₃ wt.%) and 0.029 Gd apfu (2.18 Gd₂O₃ wt.%), as well as in a more compositionally varied monazite-(Sm), containing up to 0.261 Nd apfu (18.52 wt.% Nd₂O₃), 0.462 Sm apfu (33.22 wt.% Sm₂O₃) and 0.148 Gd apfu (11.05 wt.% Gd₂O₃). All monazite species exhibit significant Eu, Dy and Er concentrations, and monazite-(Ce) is also enriched in Y. The monazite-(Nd) had a composition consisting of (Nd_{0.486}Ce_{0.257}Sm_{0.095}Pr_{0.077}Gd_{0.029}La_{0.026}Eu_{0.019}Dy_{0.002}Er_{0.002}U_{0.001})(P_{0.999}Si_{0.005})O₄ (one spot analysis), while monazite-(Sm) was assigned a composition of (Sm_{0.462}Nd_{0.191}Gd_{0.148}Ce_{0.113}Pr_{0.028}La_{0.018}Eu_{0.005}Dy_{0.005}Er_{0.005}Yb_{0.002}Ca_{0.012}Th_{0.010})(P_{0.996}Si_{0.007})O₄ in the portion richest in Sm.

Chondrite-normalised REE patterns (REE_{CN}) show continuously decreasing concentrations of La and Ce from monazite-(Ce), through monazite-(Nd), to monazite-(Sm); similar concentrations of Pr, Nd and Eu were observed in monazite-(Ce) and monazite-(Sm), with a distinct enrichment of these elements in monazite-(Nd) and increasing concentrations of Sm and Gd from monazite-(Ce) to monazite-(Sm) (Fig. 2). Monazite-(Sm) and monazite-(Ce) are characterised by a negative Eu anomaly, whereas the REE pattern of monazite-(Nd) reveals no Eu anomaly. The decomposition of the REE_{CN} patterns of monazite-(Sm) and monazite-(Ce) was made with the *BlambdaR* application (Anenburg and Williams, 2022) for two populations of λ and τ coefficients: (1) ($\lambda_0, \lambda_1, \lambda_2, \lambda_3, \lambda_4$) and ($\tau_1, \tau_2, \tau_3, 0$) and (2) ($\lambda_0, \lambda_1, \lambda_2, \lambda_3, 0$) and ($\tau_1, \tau_2, \tau_3, 0$) with the considered Eu anomaly, leading to optimal values of $r^2 > 0.99$ and χ^2 in the range of 1.6–18.7 for $s = 0.05$ (Table S2). The symbol '0' in place of λ_4 and τ_4 denotes that the coefficients were excluded from the fitting procedure, e.g. the tetrad effect τ_4 was not fitted due to the lack or scarcity of analytical data for elements ranging from Er to Lu. The REE_{CN} pattern of the monazite-(Nd) was fitted with the ($\lambda_0, \lambda_1, \lambda_2, \lambda_3, \lambda_4$) and (0, 0, $\tau_3, 0$) coefficients without a considered Eu anomaly, which led to the best statistical parameters of $r^2 > 0.998$ and $\chi^2 = 2.46$ for the assumed s value (Table S2). The negative Eu anomaly,

Table 1. Representative compositions of monazite-group minerals in the Blue Beryl Dyke.

Specimen No.	P220	P235	P236	P219	P219		P220	P235	P236	P219	P219
<i>N</i>	11	4	9	4	8	Apfu	11	4	9	4	8
Wt.%	Mnz-Ce	Mnz-Ce	Mnz-Nd	Mnz-Sm	Mnz-Sm		Mnz-Ce	Mnz-Ce	Mnz-Nd	Mnz-Sm	Mnz-Sm
P ₂ O ₅	29.11	28.54	29.58	29.15	28.86	P ⁵⁺	0.980	0.958	0.999	0.996	0.987
SiO ₂	0.57	1.12	0.12	0.18	0.36	Si ⁴⁺	0.022	0.044	0.005	0.007	0.014
ThO ₂	2.58	14.91	0.00	1.11	1.93	Th ⁴⁺	0.023	0.135	0.000	0.010	0.018
UO ₂	b.d.l.	0.98	0.15	b.d.l.	b.d.l.	U ⁴⁺	0.000	0.009	0.001	0.000	0.000
Y ₂ O ₃	0.24	0.48	b.d.l.	b.d.l.	b.d.l.	Y ³⁺	0.005	0.010	0.000	0.000	0.000
La ₂ O ₃	4.20	4.64	1.73	1.21	0.95	La ³⁺	0.062	0.068	0.026	0.018	0.014
Ce ₂ O ₃	23.26	18.85	17.56	7.62	9.75	Ce ³⁺	0.338	0.274	0.257	0.113	0.144
Pr ₂ O ₃	3.94	2.69	5.31	1.88	2.46	Pr ³⁺	0.057	0.039	0.077	0.028	0.036
Nd ₂ O ₃	19.19	12.81	34.12	13.25	16.92	Nd ³⁺	0.272	0.181	0.486	0.191	0.244
Sm ₂ O ₃	11.07	7.68	6.90	33.22	29.50	Sm ³⁺	0.152	0.105	0.095	0.462	0.411
Eu ₂ O ₃	0.85	0.64	1.38	0.38	0.54	Eu ³⁺	0.012	0.009	0.019	0.005	0.007
Gd ₂ O ₃	4.58	4.03	2.18	11.06	7.69	Gd ³⁺	0.060	0.053	0.029	0.148	0.103
Dy ₂ O ₃	0.10	0.22	0.14	0.37	0.15	Dy ³⁺	0.001	0.003	0.002	0.005	0.002
Er ₂ O ₃	0.85	0.64	0.19	0.38	0.54	Er ³⁺	0.011	0.008	0.002	0.005	0.007
Yb ₂ O ₃	b.d.l.	b.d.l.	b.d.l.	0.16	0.15	Yb ³⁺	0.000	0.000	0.000	0.002	0.002
CaO	0.11	2.43	0.00	0.27	0.26	Ca ²⁺	0.005	0.103	0.000	0.012	0.011
PbO	b.d.l.	0.18	b.d.l.	b.d.l.	b.d.l.	Pb ²⁺	0.000	0.002	0.000	0.000	0.000
Total	100.65	100.84	99.37	100.23	100.06	Σan.	1.002	1.003	1.004	1.003	1.002
						Σcat.	0.998	0.998	0.994	0.998	1.000

Notes: b.d.l. – below detection limit; Σan. (cat.) – total of anions (cations); *N* = number of spot analysis.

Eu_{CN}/Eu_{λ_T} in the REE_{CN} patterns of monazite-(Sm) varied from 0.03–0.09 [average 0.06(2)], those of monazite-(Ce) from 0.22–0.49 [average 0.33(12)], and in the case of monazite-(Nd), which did not reveal a clear Eu anomaly, the value was estimated at 0.97 on the basis of fitting with the *BlambdaR* application.

Genetic implications

To the best of our knowledge, the monazite-(Nd) and monazite-(Sm) from Piława Górna are the two most Nd- and Sm-enriched crystals worldwide. This could imply that these elements, with abundances in the Earth's continental crust of ~20 and 3.9 ppm, respectively (Rudnick, 2018), have been concentrated by ~1.5×10⁴ times in monazite-(Nd) and from up to 8×10³ times (Nd) to above 70×10³ times (Sm) in monazite-(Sm). Thus, it is clear that geochemical fractionation of REE itself within a bulk volume of the pegmatite-forming melt was not the only crucial factor for the chemical composition of these crystals. When explaining the crystal-chemistry of monazite-(Gd), Ondrejka *et al.* (2023) suggested the role of a localised process in a chemically near-closed system leading to the progressive concentration of MREE in fluids as a result of the promoted crystallisation of early monazite-(Ce) and xenotime-(Y), which selectively decreased the LREE and HREE contents in the crystallisation environment. The abnormally high Sm- and Nb-enrichment of the Blue Beryl Dyke monazite-(Sm) and monazite-(Nd), and exceptional rarity of these monazite species in the dyke also suggest local REE geochemical anomalies in the pegmatite-forming melt–fluid system related to variations of its chemical and physical parameters, even at the micro scale. These led to the rapid growth of accessory phases under supercooling conditions which scavenged selected elements leading to their local depletion that was not balanced by diffusion processes. We suggest that the outstripping crystallisation of xenotime-(Y) progressively increased the local abundances of LREE (Gd to La), first enabling the occasional crystallisation of monazite-(Sm) with a large negative Eu anomaly; this then led to the crystallisation of (Sm,Nd)-bearing monazite-(Ce) with greater Eu³⁺ concentrations than in the monazite-(Sm), and finally to the formation of

monazite-(Nd) with a smooth REE_{CN} pattern. As is known, the main reason for the Eu anomaly is in the presence of Eu²⁺ or Eu³⁺ species in the crystallisation environment (Weill and Drake, 1973; Bau, 1991; Deer *et al.*, 2001). At higher temperatures and in more reducing magmas, Eu occurs as Eu²⁺ which is compatible with Ca-bearing melt components, mainly becoming incorporated into plagioclase crystals. At lower temperatures and under more oxidising conditions, the element will occur as Eu³⁺, becoming incompatible with the melt components but compatible with other trivalent REE. Thus, the decreasing negative Eu anomaly in monazite-(Sm) through monazite-(Ce) to monazite-(Nd) [from 0.06(2) to 0.33(12) and 0.97, respectively] indicates increasing amounts of Eu³⁺ in probably more oxidising fluids coexisting with the pegmatite-forming melt, which were subsequently remobilised by the coeval local hydrothermal alteration of plagioclase. The fluid also affected the REE fractionation, decreasing the tetrad effect on the third, second, and first tetrads. These observations provide additional insights into the evolution of the crystallisation environment of the monazites.

Monazite-(Sm) exhibiting a negative Eu anomaly has been found as an intergrowth with partly digested columbite-(Mn) undergoing alteration to fluor- and oxy/hydroxycalciumicrolite and finally to F-free plumbomicrolite associated with ferrowodginite, wodginite, F-bearing tourmaline, fluorapatite and Cs-bearing mica. This indicates relatively early crystallisation of the mineral from a pegmatite-forming melt evolving into a residual melt coexisting with aqueous fluids. High-temperature hydrothermal fluids are commonly associated with the presence of strong REE-complexing ligands such as F⁻, Cl⁻, OH⁻, and PO₄³⁻, which are reported to be the most effective agents in the mobilisation, transport, fractionation, and deposition of REE species (Gieré, 1990; Jiang *et al.*, 2005; Migdisov and Williams-Jones, 2014; Williams-Jones, 2015; Migdisov *et al.*, 2016). Among these anions, Cl⁻ forms the weakest complexes with REE and F⁻ the strongest ones (Migdisov *et al.*, 2016). However, as chloride is a dominant ligand in natural hydrothermal systems, it is mainly responsible for hydrothermal transport of the REE. Thus, Nd and Sm may have undergone additional fractionation within the

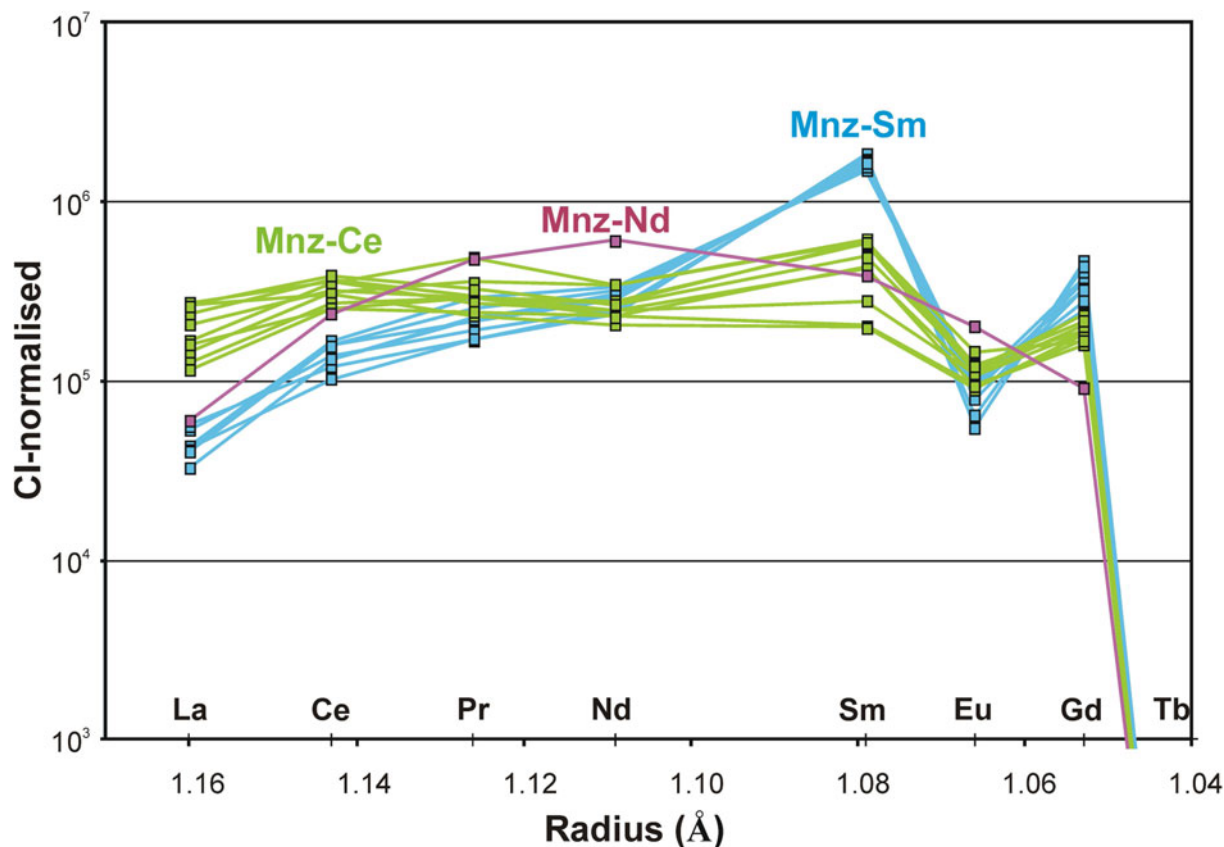


Figure 2. REE patterns of monazite-group minerals from the Blue Beryl Dyke normalised to the CI chondrite (O'Neill, 2016).

Blue Beryl Dyke during the hydrothermal stage due to the different stabilities of LREE-chloride complexes, and differences in their mobility and solubility. This fractionation should decrease with increasing atomic number of the REE, which was corroborated in the Blue Beryl Dyke monazites by the decreasing tetrad effect on the third, second, and first tetrads from monazite-(Sm) through monazite-(Ce) to monazite-(Nd). Due to significant differences between the stability/mobility of LREE-chloride complexes and those involving HREE, this process may have led to Sm- and Nd-enrichment resulting in the local saturation in SmPO_4 and NdPO_4 at different stages of the system's evolution. The destabilisation of Nd-Cl and Sm-Cl complexes could also have been related to the neutralisation of the solution's acidity, e.g. through F consumption during the formation of F-bearing tourmaline, fluorapatite, or fluor-calcium microlite.

In melt-fluid systems, Th and U, the two elements that are commonly associated with REE in monazite-group minerals, are highly compatible. Among the studied monazite crystals, monazite-(Ce) was the most enriched in Th and U, containing up to 14.91 wt.% ThO_2 and 1.76 wt.% UO_2 . The amounts of ThO_2 in monazite-(Sm) were <2 wt.% and UO_2 was absent altogether; in turn, small amounts of UO_2 were measured in monazite-(Nd) (0.15 wt.%), whereas ThO_2 was absent. According to Keppler and Wyllie (1990, 1991), the Th and U partitioning coefficients between fluid and melt are very low if water is the only volatile component present. However, this partitioning increases significantly as the F^- concentration increases, indicating the extraction of certain amounts of Th and U from the melt through the formation of fluoride complexes in the fluid.

Chloride anions may form complexes with U, but not with Th; the latter will not be extracted under such conditions. Consequently, fluids with higher Cl^- concentrations coexisting with more peraluminous silicate melts will reduce the initial U contents of the melts as the latter will partition into the fluid phase. These data on the behaviours of Th and U in melt-fluid systems corroborate the crystallisation of monazite-(Sm) from a melt which became progressively enriched in volatiles, including F and Cl. The system evolved progressively into a hydrated F-bearing residual melt from which the (Sm,Nd)-bearing monazite-(Ce) crystallised and which lost U through the formation of (U-Cl)-complexes in the fluid. Monazite-(Nd), occurring as $\sim 10 \mu\text{m}$ inclusions in columbite-(Fe), had a different REE_{CN} pattern shaped by λ coefficients that differed from those characteristic of monazite-(Sm) and monazite-(Ce); this monazite also had the weakest tetrad effect only on the third tetrad, and a negligible Eu anomaly. The small UO_2 contents and the absence of ThO_2 as well as its coexistence with inclusions of other phases crystallised from fluids (cassiterite, scheelite, uraninite and a BiVO_4 phase) indicate late crystallisation from fluids devoid of fluorine, which potentially could be coeval with the formation of F-free oxy/hydroxy-plumbomicrolite, as well as possible formation through secondary remobilisation and *in situ* crystallisation. These data agree with the observations of Gysi *et al.* (2018) who showed that the REE_{CN} profiles of monazites could be classed into two groups based on their LREE contents: one group showing the limited fractionation of La, Ce, Pr and Nd, and the other group showing a strong geochemical fractionation and including enhanced concentrations of Sm, Eu and Gd. These authors

explained the differentiation as resulting from the incorporation of REE with varying ionic radii to match the geometric parameters of the monazite structure.

Conclusions

The presence of highly fractionated accessory mineral phases such as monazite-(Sm) and monazite-(Nd) in the pegmatites described here resulted from the interaction of several factors. The most important of these appear to be:

The presence of highly fractionated pegmatite melts and hydrothermal fluids during the final stages of pegmatite solidification, which were enriched in REE and other metals in the form of complexes mainly with Cl^- , F^- , and OH^- ligands.

A very rapid growth of all accessory phases under supercooling conditions which scavenged selected elements leading to their local depletion in the melt. On the scale of the bulk pegmatite body, this process strongly differentiated the local concentrations of these elements, which were not subsequently balanced by diffusion processes.

The crystallisation of pegmatite-forming melts under supercooling conditions forced the growth of accessory phases that consumed elements that were available in the local environment, and which could occupy acceptable structural positions within the structures of the crystallising phases.

Acknowledgements. We thank Monika A. Kusiak and Martin Ondrejka for helpful and constructive comments and suggestions, which greatly improved the manuscript. We are also very grateful to Sam Broom-Fendley for language corrections. This study was supported by AGH University of Science and Technology grant 16.16.140.315.

Supplementary material. The supplementary material for this article can be found at <https://doi.org/10.1180/mgm.2023.38>.

Competing interests. The authors declare none.

References

- Anenburg M. and Williams M.J. (2022) Quantifying the tetrad effect, shape components, and Ce–Eu–Gd anomalies in rare earth element patterns. *Mathematical Geosciences*, **54**, 47–70.
- Bau M. (1991) Rare-earth element mobility during hydrothermal and metamorphic fluid-rock interaction and the significance on the oxidation state of europium. *Chemical Geology*, **93**, 219–230.
- Černý P. and Ercit T.S. (2005) The classification of granitic pegmatites revisited. *The Canadian Mineralogist*, **43**, 2005–2026.
- Deer W.A., Howie R.A. and Zussman J. (2001) *Rock-Forming Minerals, vol. 4A, Framework Silicates: Feldspars*. 2nd ed, The Geological Society, London.
- Del Blanco M., Costas Ulbrich M., Echeveste H. and Vlach S.R.F. (1998) Las monacitas-(Nd) con samario de los diques carbonatíticos del sector nororiental de la Sierra de Cobres, Salta, Argentina. *IV Reunión de Mineralogía y Metalogía, Universidad Nacional del Sur – Bahía Blanca*. MINMET'98–EDIUNS, pp. 63–69.
- Gieré R. (1990) Hydrothermal mobility of Ti, Zr and REE: examples from the Bergell and 612 Adamello contact aureoles (Italy). *Terra Nova*, **2**, 60–67.
- Graeser S. and Schwander H. (1987) Gasparite-(Ce) and monazite-(Nd): two new minerals to the monazite group from the Alps. *Schweizerische Mineralogische und Petrographische Mitteilungen*, **67**, 103–113.
- Gysi A.P., Harlov D.E. and Miron G.D. (2018) The solubility of monazite (CePO_4), SmPO_4 , and GdPO_4 in aqueous solutions from 100 to 250 °C. *Geochimica et Cosmochimica Acta*, **242**, 143–164.
- Jiang S.Y., Wang R.C., Xu X.S. and Zhao K.D. (2005) Mobility of high field strength elements (HFSE) in magmatic-, metamorphic-, and submarine-hydrothermal systems. *Physics and Chemistry of the Earth*, **30**, 1020–1029.
- Keppeler H. and Wyllie P.J. (1990) Role of fluids in transport and fractionation of uranium and thorium in magmatic processes. *Nature*, **348**, 531–533.
- Keppeler H. and Wyllie P.J. (1991) Partitioning of Cu, Sn, Mo, W, U, and Th between melt and aqueous fluid in the systems haplogranite– H_2O –HCl and haplogranite– H_2O –HF. *Contribution to Mineralogy and Petrology*, **109**, 139–150.
- Kusiak M.A. and González-Álvarez I. (2006) Nd-monazite occurrence in North America: mesoproterozoic siliciclastic rocks of the Belt–Purcell Supergroup. *Geochimica et Cosmochimica Acta*, **70**, 18.
- Levinson A.A. (1966) A system of nomenclature for rare-earth minerals. *American Mineralogist*, **51**, 152–158.
- Linthout K. (2007) Tripartite division of the system 2REEPO_4 – $\text{CaTh}(\text{PO}_4)_2$ – 2ThSiO_4 , discreditation of brabantite, and recognition of cheralite as the name for members dominated by $\text{CaTh}(\text{PO}_4)_2$. *The Canadian Mineralogist*, **45**, 503–508.
- Masau M., Černý P., Cooper M.A. and Chapman R. (2002) Monazite-(Sm), a new member of the monazite group from the Annie Claim #3 granitic pegmatite, Southeastern Manitoba. *The Canadian Mineralogist*, **40**, 1649–1655.
- Migdisov A. and Williams-Jones A.E. (2014) Hydrothermal transport and deposition of the rare earth elements by fluorine-bearing aqueous liquids. *Mineralium Deposita*, **49**, 987–997.
- Migdisov A., Williams-Jones A.E., Brugger J. and Caporuscio F.A. (2016) Hydrothermal transport, deposition, and fractionation of the REE: Experimental data and thermodynamic calculations. *Chemical Geology*, **439**, 13–42.
- Mitchell R.H. and Smith D.L. (2017) Geology and mineralogy of the Ashram Zone carbonatite, Eldor Complex, Dubec. *Ore Geology Reviews*, **86**, 764–806.
- Ondrejka M., Uher P., Ferenc Š., Milovská S., Mikuš T., Molnárová A., Škoda R., Kopáček R. and Bačík P. (2023) Gadolinium-dominant monazite and xenotime: selective hydrothermal enrichment of middle REE during low-temperature alteration of uraninite, brannerite and fluorapatite (the Zimná Voda REE-U-Au quartz vein, Western Carpathians, Slovakia). *American Mineralogist*, **108**, 754–768.
- O'Neill H.St.C. (2016) The smoothness and shapes of chondrite-normalized rare earth element patterns in basalts. *Journal of Petrology*, **57**, 1463–1508.
- Pieczka A., Szuszkiewicz A., Szełęg E., Janeczek J. and Nejbert K. (2015) Granitic pegmatites of the Polish part of the Sudetes (NE Bohemian massif, SW Poland). *Fieldtrip Guidebook C. 7th International Symposium on Granitic Pegmatites*, Książ, Poland, pp. 73–103.
- Pieczka A., Gołębiowska B., Jeleń P., Włodek A., Szełęg E. and Szuszkiewicz A. (2018) Towards Zn-dominant tourmaline: a case of Zn-rich fluor-elbaite and elbaite from the Julianna system at Piława Górna, Lower Silesia, SW Poland. *Minerals*, **8**, 126.
- Pieczka A., Szełęg E. and Szuszkiewicz A. (2019) *Pegmatyty Dolnego Śląska (Pegmatites of Lower Silesia)*. AGH University of Science and Technology, Kraków [in Polish only].
- Pouchou J.L. and Pichoir F. (1991) Quantitative analysis of homogeneous or stratified microvolumes applying the model "PAP". Pp. 31–75 in: *Electron Probe Quantitation* (K.F.J. Heinrich and D.E. Newbury DE, editors). Plenum Press, New York, USA.
- Pršek J., Ondrejka M., Bačík P., Budzyń B. and Uher P. (2010) Metamorphic-hydrothermal REE minerals in the Bacúch magnetite deposit, Western Carpathians, Slovakia: (Sr, S)-rich monazite-(Ce) and Nd-dominant hingganite. *The Canadian Mineralogist*, **48**, 81–94.
- Reed S.J.B. and Buckley A. (1998) Rare-earth element determination in minerals by electron-probe microanalysis: application of spectrum synthesis. *Mineralogical Magazine*, **62**, 1–8.
- Rudnick R.L. (2018) Earth's continental crust. In: *Encyclopedia of Geochemistry* (White, W.M. editor). Encyclopedia of Earth Sciences Series. Springer, Cham. https://doi.org/10.1007/978-3-319-39312-4_277.
- Števkó M., Uher P., Ondrejka M., Ozdín D. and Bačík P. (2014) Quartz–apatite–REE phosphates–uraninite vein mineralization near Čučma (eastern Slovakia): a product of early Alpine hydrothermal activity in the Gemeric Superunit, Western Carpathians. *Journal of Geosciences*, **59**, 209–222.
- Szuszkiewicz A., Szełęg E., Pieczka A., Ilnicki S., Nejbert K., Turniak K., Banach M., Łodziński M., Różniak R. and Michałowski P. (2013) The Julianna pegmatite vein system at the Piława Górna mine, Góry Sowie Block, SW Poland – preliminary data on geology and descriptive mineralogy. *Geological Quarterly*, **57**, 467–484.

- Timmermann H., Parrish R.R., Noble S.R. and Kryza R. (2000) New U–Pb monazite and zircon data from the Sudetes Mountains in SW Poland: evidence for a single-cycle Variscan Orogeny. *Journal of the Geological Society*, **157**, 265–268.
- Van Breemen O., Bowes D.R., Aftalion M., and Żelaźniewicz A. (1988) Devonian tectonothermal activity in the Sowie Góry gneissic block, Sudetes, southwestern Poland: evidence from Rb–Sr and U–Pb isotopic studies. *Journal of Polish Geological Society*, **58**, 3–10.
- Warr L.N. (2021) IMA–CNMNC approved mineral symbols. *Mineralogical Magazine*, **85**, 291–320.
- Weill D.F. and Drake M.J. (1973) Europium anomaly in plagioclase feldspar: experimental results and semiquantitative model. *Science*, **180**, 1059–1060.
- Williams-Jones A.E. (2015) The hydrothermal mobility of the rare earth elements. Pp. 119–123 in: *Symposium on Strategic and Critical Materials Proceedings* (Simandl, G.J. and Neetz, M., editors). British Columbia Geological Survey Paper 2015-3. British Columbia Ministry of Energy and Mines, Canada.
- Wise M.A., Müller A. and Simmons W.B. (2022) A proposed new mineralogical classification system for granitic pegmatites. *The Canadian Mineralogist*, **60**, 229–248.